This paper can be found at https://doi.org/10.1016/j.jclepro.2020.124783

Compressed Earth Blocks Stabilised with Glass Waste and Fly Ash Activated with a Recycled Alkaline Cleaning Solution

[a] Jhonathan Rivera; [b] João Coelho; [c] Rui Silva; [d] Tiago Miranda; [e] Fernando Castro; [f,*] Nuno Cristelo

[a] CQ-VR, Department of Engineering, University of Trás-os-Montes e Alto Douro, Quinta de Prados, 5000-801 Vila Real, Portugal
E-mail address: jhonathan@utad.pt

[b] Department of Civil Engineering, University of Minho, 4800-058 Guimarães, Portugal
E-mail address: id7225@uminho.com

[c] ISISE, Department of Civil Engineering, University of Minho, 4800-058 Guimarães, Portugal
E-mail address: ruisilva@civil.uminho.com

[d] ISISE, Institute of Science and Innovation for Bio-Sustainability (IB-S), Department of Civil Engineering, University of Minho, 4800-058 Guimarães, Portugal
E-mail address: tmiranda@civil.uminho.com

Portugal
E-mail address: fcastro@w2v.pt

[f] CQ-VR, Department of Engineering, University of Trás-os-Montes e Alto Douro, Quinta de Prados, 5000-801 Vila Real, Portugal
E-mail address: ncristel@utad.pt
[*] Corresponding author

Abstract

The study reported in this paper focused on the physical-mechanical properties of compacted earth blocks (CEB) stabilised with a sustainable alkali activated cement, completely produced from wastes and residues, including coal fly ash and glass waste (from the production of ophthalmic lenses) activated with an alkaline solution resulting from the aluminium industry. A common Portuguese silty clay was used as the mineral skeleton of the blocks, which were then evaluated based on the protocols of the UNE 41410 and DIN 18945-47 standards. The results evidenced the effectiveness of the alkaline cementing agent in forming a binding matrix for the soil particles, and the resulting material was used to manufacture the earth-based masonry elements. After a careful optimisation of the sustainable binder, an average compressive strength of 17.23 MPa, in unsaturated conditions, was obtained for the blocks. The newly formed soil-binder structure was very capable to withstand wetting and drying cycles, ice-thaw cycles and erosion. The microstructure of the material was further analysed, using scanning electron microscopy and energy dispersive spectroscopy. The results demonstrated the real possibility of using this type of cement as a viable alternative to traditional soil stabilisation binders used in earth construction.

Key words: Alkali activated cements; sustainability; earth construction; soil stabilisation; glass waste

1. Introduction

For millennia compacted earth has been one of the most used materials around the world, mostly for housing construction, using two techniques known as "rammed earth" and "adobe". Rammed earth is a thick wall of soil rammed inside a wooden formwork, while adobe is formed by blocks of compressed soil, usually slightly larger than a clay brick, they may or may not include reinforcing fibres. Compacted earth blocks (CEB) are considered an evolution from adobe (Pacheco-Torgal and Jalali, 2012), since the manufacturing follows the same principle, only the compaction process has been improved and, additionally, chemical stabilization is applied, thus improving mechanical properties and durability. The compaction technique has also evolved, from the appearance of the first CINVA-RAM compactor machine, to the current use of hydraulic presses, capable of significantly improving the geometry and material properties of the CEB (Silva et al., 2015).

The chemical stabilization of soils to manufacture CEB is traditionally done with Portland cement (OPC) or lime. However, in some cases, these traditional cements are not a viable solution due to the financial cost of the material, if high cement contents are required to obtain adequate properties. Therefore, it is justifiable to research alternative binders, preferably capable of producing a more environmentally friendly material. In that context, alternative binders based on industrial wastes or by-products are gaining acceptance, thus becoming ideal for this particular application. From a relatively large pool of possibilities, fly ash (FA) is a clear target, due to its extensive research in the last 20 years, which includes applications as a soil stabilizer and as a precursor in alkaline activation reactions. This residue from the combustion of coal, in thermoelectric powerplants, can act as a soil filler, reducing the settlement of the resulting material, or can also be used together with a source of calcium, taking advantage of its pozzolanic properties (Horpibulsuk et al., 2009; Siddiqua and Barreto, 2018).

Slags are also one of the most used wastes in this type of applications, and especially ground granulated blast furnace slags (GGBS), because of its high content in calcium oxides and hydraulic character, that makes them very similar to OPC. Oti et al. (2009a, 2009b) used mixtures of GGBS and quick lime or hydraulic lime to stabilize a clayey soil, which was then compacted with a hydraulic press to produce CEB. The GGBS/lime binder improved compressive strength and especially the durability, in terms of ice/thaw cycles. Mixtures of GGBS and OPC showed less effective results, which was attributed to the increased cationic exchange capacity between the soil and the lime-based binder. In addition to FA and GGBS, it is also worth mentioning the successful use, as chemical stabilizers for the manufacture of BTC, of ashes from sugarcane bagasse and marble stone cutting muds. El-Mahllawy et al. (2018) and Lima et al. (2012) mixed this type of waste with OPC and lime, in varied percentages, effectively improving properties such as compressive strength and absorption of the CEB.

Glass wastes (GW) are used, since the 1970s, in the manufacture of baked bricks. Due to its very specific composition, they function as a melting material in the sintering process of clay minerals (Hwang et al., 2006; Zhang et al., 2018). However, the use of glass waste as a chemical stabilizer in the manufacture of BTC is not possible, because it is completely inert if not in contact with a strong alkaline substance or a high acidic medium. Therefore, in geotechnics, they are used mostly as a filler material, as a plasticity modifier or to increase the internal friction angle of clay soil particles (Olufowobi et al., 2014). In order to improve and use glass wastes as cementing materials, methods such as alkaline activation are showing significant potential, mostly due to the capacity of the alkaline activators, mainly alkali metal salts, to dissolve the previously pulverized glass. Several authors (Avila-López et al., 2015; Espinoza and Escalante García, 1970; Lin et al., 2012; Novais et al., 2016; Pascual et al., 2014; Rivera et al., 2018) have successfully used alkaline activated glass waste as a cementitious material in various applications, demonstrating that pulverized glass waste can be an alternative to traditional Portland cements, either when used as the sole precursor or mixed with other aluminosilicate-rich precursors.

The alkaline activation technique is no stranger to the development of masonry elements made of raw earth. This technique, combined with precursor residues or commercial aluminosilicates, such as metakaolin, have been used to chemically stabilize soils for subsequent compaction and manufacture of BTC. Very interesting results have been obtained (Leitão et al., 2017; Omar Sore et al., 2018; Silva et al., 2015), showing the capacity of the technique to greatly improve the mechanical properties, durability and stability in water of the compacted elements; and even acquire properties comparable to the BTC stabilized with OPC. Furthermore, a step forward was already given towards the implementation of alternative, more environmentally friendly activators, with an optimised incorporated energy, with the purpose of producing masonry with a very low carbon footprint. Recent research (Cristelo et al., 2019; Fernández-Jiménez et al., 2017) has shown that the use of glass waste, combined with precursors like fly ash and aluminium anodizing sludge, activated with a recycled alkaline cleaning solution, can originate a sustainable alkaline cement.

In the present work, the physical-mechanical characterization of chemically stabilized CEB was carried out, integrating various types of industrial waste into the soil stabilization process and manufacturing of the CEB, with the intention of replacing traditional precursors, such as blast furnace slag or metakaolin, and alkaline activators such as hydroxides or silicates.

2. Materials and methods

2.1 Materiales

The soil was collected in the area of Chaves, a city in the Northern Region of Portugal. The fly ash was generated by the Portuguese thermo-electric powerplant of Pego. According to ASTM C618 (2012), it was classified as a class F. The glass waste powder results from the production of optical lenses at the Portuguese company POLO. The chemical composition of the soil and precursors is presented in Table 1, obtained by x-ray fluorescence with a PHILLIPS PW-1004 spectrometer.

The recycled cleaning solution acting as the alkaline activator has a high pH, between 12 and 14, with an approximate density of 1.3 g/cm^3. It previously underwent a homogenization process. Table 2 shows the elementary composition of the cleaning solution, determined by Inductively Coupled Plasma Atomic Emission Spectrometer (ICP-AES), with plasma power of 1.4 kW, plasma gas flow of 15.00 l / min and gas nebulizer flow of 0.85 l/min, with a reading time of 5s.

Table 1. Chemical composition of the Fly ash, Soil and Waste glass (%w)

Element (oxides)	Fly ash	Soil	Waste glass
SiO_2	56.11	61.74	58.37
Al_2O_3	21.44	23.27	3.94
Fe_2O_3	8.20	5.68	0.15
CaO	1.31	0.33	6.13
MgO	1.46	1.65	0.49
TiO_2	1.15	0.08	-
MnO	0.07	0.89	2.73
Na_2O	1.12	0.58	8.75
K_2O	2.81	5.12	4.66
P_2O_5	0.29	0.09	5.07
LOI	5.05	0.33	1.85

Table 2. Elemental composition of the cleaning solution

Al_2O_3	Na_2O	SO_3	H_2O	pH	[a]$[OH]^-$	Density (g/cm^3)
7.14	12.13	1.18	79.5	12-14	5.3	1.30

[a] Acid-base reaction with 5 N HCL (Panrea S.A.)

Figure 1 shows the particle size distribution of the soil and both precursors. The curves were obtained by laser diffraction, using a Sympatec Helos BF particle size analyser, with a measuring range between 0.9 mm and 175 mm. The particle size below 45µm was 75.6, 81.3 and 99.2% for fly ash, soil and glass waste, respectively.

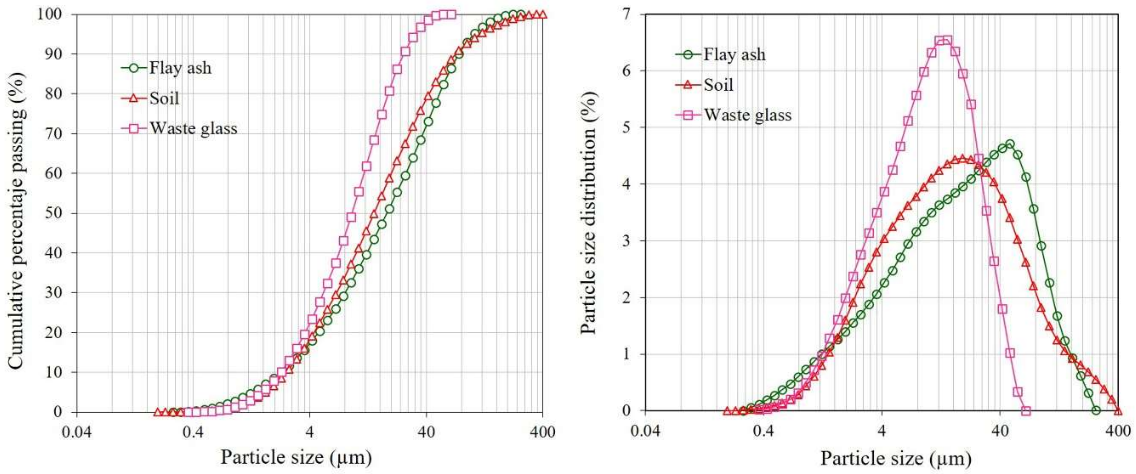

Figure 1. Cumulative particle size and particle size distribution of the Fly ash, Soil and Waste glass

The mineralogical composition of the soil and precursors and the soil was determined using X-ray diffraction (XRD), with a PANAlytical X'Pert Pro MPD, with CuKα radiation at 40Kev and 30mA, equipped with a detector X´Celerator and a secondary monochromator. The diffractograms are presented in Figure 2. The glass residue is a highly amorphous material, as evidenced by the large halo between the 17°(2θ) to 37°(2θ) angles. The fly ash is a semi-crystalline material, also with some amorphous content, represented by a smaller halo between angles 18°(2θ) and 32°(2θ). It is mineralogy composed essentially by quartz, mullite and hematite. As expected, the soil is a totally crystalline material, composed of several minerals such as quartz, kaolinite magnetite and albite.

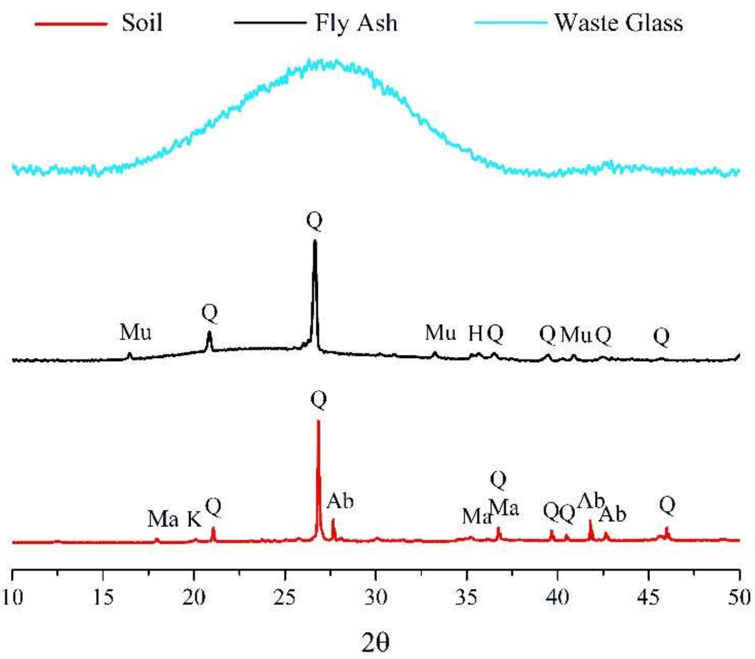

Figure 2. XRD Pattern of the original materials . Fly ash: Mu=Mullite, Q= quartz, H=Hematite; Soil: Q=quartz, K=Kaolinite, Ma=Magnetite, Ab= Albite

2.2 Definition of the alkaline cement

Prior to the stabilization of the soil, it was necessary to define the composition of the alkaline activated cement (AAC) that would be used as a binder. This AAC was prepared with the described cleaning solution (CS), which was used to activate the glass waste (GW) and the fly ash (FA), acting as the precursor, in a 50/50 weight ratio. The CS was added according with pre-defined activator/precursor weight ratios of 0.50, 0.57 and 0.75. The lowest of these values was defined based on the minimum workability requirements. The pastes were then moulded in 4 cm cubic specimens, which were cured at 50ºC and 10% relative humidity in a climatic chamber, for 7 days. Figure 3 presents the uniaxial compressive strength (UCS) obtained by each of the AAC tested. The highest UCS (11.6 MPa) was obtained with the lower activator/precursor ratio of 0.50.

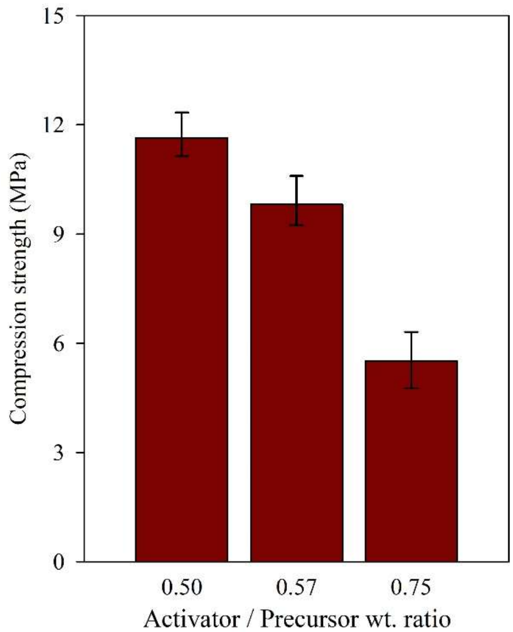

Figure 3. Compressive strength, after 7 days curing, of the 50% FA + 50% GW precursor paste

2.3 Definition of the AAC/soil composition

To define the most adequate activator content, in terms of dry density, a Standard Proctor test was carried out based on the methodology proposed by the EN13286-42 (2004), using the AAC with an activator/precursor ratio of 0.50 as a starting point. The test was performed with 3 layers and 12 blows per layer, on pastes with a precursor/soil weight ratio of 30/70. A curve was obtained (Figure 4) by adding more or less activator to the solids (precursor + soil), from which the maximum dry density and optimum moisture content were identified as 1.77 g/cm^3 and 17%, respectively.

However, when the CEB was compacted, significant expansion was registered, which was attributed to excessive moisture. To avoid this effect during the fabrication of the CEB, it was decided to further optimise the moisture content in the AAC/soil composition, aiming at a value lower than 17%, without reducing the density of 1.77 g/cm^3 obtained during the Proctor test. This was possible due to the higher energy applied by the earth block compaction machine, compared with the dynamic energy transmitted by the Proctor hammer.

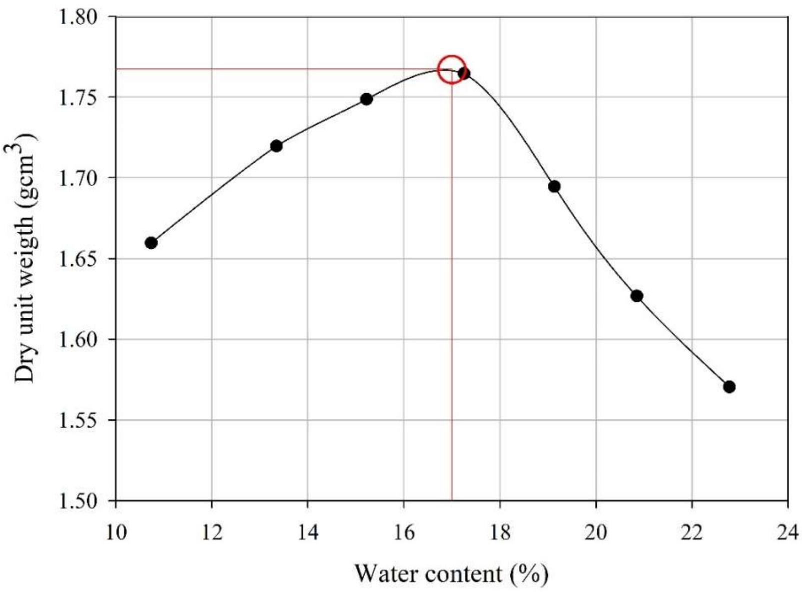

Figure 4. Proctor test results for the stabilised soil, using the activator as the liquid phase and a precursor/soil weight ratio of 30/70

This optimisation was developed through an experiment design based on the response surface methodology (RSM). A Central Composite Design (CCD) was configured with the aim of finding a relation between the independent variables and the response variable (compressive strength) capable of maximize the latter (Montgomery and Runger, 2014), therefore defining the most effective AAC/soil combination. Table 3 presents the independent variables considered (i.e. soil/precursor and activator/solids), as well as their respective range. The commercially available software *Minitab 17* was used which, based on the number of independent variables assumed, established a total of 13 random runs. The soil/precursor range was defined based on previous experience by the research team (Corrêa-Silva et al., 2019; Cristelo et al., 2018; Miranda et al., 2017; Rios et al., 2016); while the activator/solid range was defined after the maximum and minimum CS content in the paste that presented the most adequate workability. This range was on the ‘dry side’ of the Proctor curve, thus below the 17% humidity threshold that produced the expansion of the paste. The response variable was assessed through compressive strength tests on compacted specimens with 70 mm in diameter and 140 mm in height, cured at 20 ± 1 °C for 28 and 180 days.

The influence of each independent variable and the corresponding compressive strength is presented in Figure 5. For the 28-day curing period, higher UCS were attained when the pastes showed the highest CS content, regardless of the precursor content; while for 180-day period the higher UCS was recorded when the CS and precursor contents simultaneously assumed their higher values.

Table 3. Definition of the independent variables and corresponding value range

Variable	Level	Value
Activator/Solids	Lower (-)	0.12
	Upper (+)	0.25
	Central Point	0.18
Soil/Precursor	Lower (-)	2.3
	Upper (+)	4.0
	Central Point	3.1

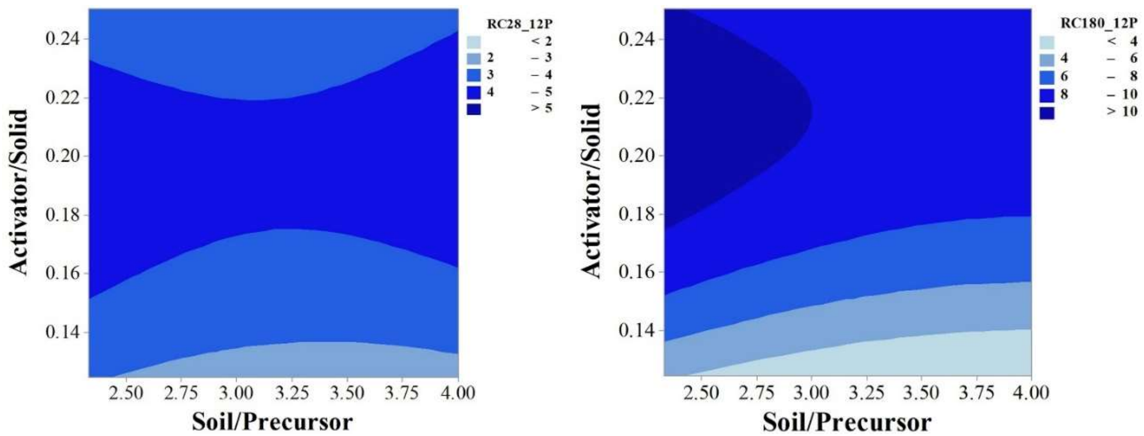

Figure 5. Contour diagrams showing the relation between the independent variables and the UCS after 28 days (left) and 180 days curing (right) on the AAC/soil

The final values of each independent variable, based on the compressive strength data of 11.4 MPa (desirability of 0.82), obtained after 180 days (Figure 6), were set at soil/precursor = 2.3 and activator/solids = 0.21.

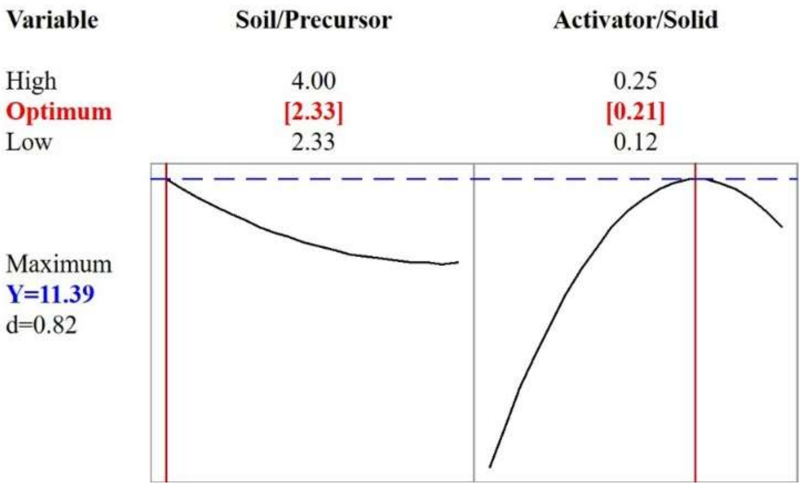

Figure 6. Optimised independent variables and resulting UCS and desirability values

2.4 Fabrication of the Compressed Earth Blocks

The CEB were fabricated with the optimised AAC-soil combination. The main steps towards the production of each block are presented in Figure 7, and involve, after a thorough mixture of the soil with the binder, the filling of two simultaneous moulds, in a fully manually operated CEB machine, their subsequent compression and, finally, the curing and drying stage. Considering that the 180-day curing result was chosen as the reference, and to avoid such prolonged waiting, the CEBs were cured at 85ºC for 20h, to accelerate the dissolution stage and the production of binding gel (Bakharev, 2005; Criado et al., 2010; Fernández-Jiménez et al., 2008, 2006; Torres-Carrasco et al., 2014; Torres-Carrasco and Puertas, 2015).

Figure 7. Main steps in the fabrication process of the CEBs, including, after mixture of the soil with the alkaline cement, the filling of the moulds (a and b), the subsequent compression (c) and the curing and drying of the resulting blocks (d)

The physical-mechanical characterization of the CEBs was carried out with compressive strength tests, water absorption tests, wetting-drying tests, ice-thawing tests and water erosion tests. Furthermore, the microstructural characterization of the AAC-soil was performed using Fourier Transform Infra-Red Spectroscopy (FTIR) and Scanning Electron Microscopy (SEM).

3. Results and discussion

3.1 Mechanical performance of the CEBs

The compressive strength is mostly accepted as a universal property to determine the quality of the CEBs. In general, the compressive strength is related to the type of soil; type and amount of stabilizer; compaction pressure and process. Table 4 summarizes the compressive strength results performed on the CEBs in both dry and saturated conditions, together with the percentage of water absorption until saturation. The maximum compressive strength reached by the CEB (17.23 MPa) was significantly higher than the uniaxial compressive strength developed by the optimum AAC/soil formulation (11.4 MPa). Such increase, of more than 50%, is not attributed to the geometry differences between the two types of specimen, but mostly to the thermal curing process that was implemented for the CEB. According to some authors (Bakharev, 2005; Singh and Subramaniam, 2019) fly ash-based alkaline cements generate mechanical strength very slowly at room temperature. On the contrary, the dissolution of the amorphous phase of the fly ash is improved if the curing occurs under an increased temperature (Rivera et al., 2018; Torres-Carrasco and Puertas, 2015), generating aluminosilicate gel in shorter periods and, thus, increasing the strength development rate of the material (Ryu et al., 2012; Šimonová et al., 2018; Singh and Subramaniam, 2019).

Table 4. Compressive strength and water absorption of the CEBs (UNE 41410, 2008)

Property		Type of specimen	
		Unsaturated CEB	*Saturated CEB*
Compressive strength (MPa)	Average	17.23	7.45
	Range	14.94 - 19.39	6.35 - 9.29
	N° of specimens	4	4
Water absortion (%)	Average	-	16.21
	Range		15.92 - 16.49
	N° of specimen		4

The UNE 41410 (2008) standard classifies the CEBs in three categories, according to its respective compressive strength: CEB1, CEB3 and CEB5. Each category corresponds to the minimum compressive strength of the CEB, e.g. category CEB5 corresponds to the blocks with a strength of at least 5 MPa. According to this standard, it is possible to classify the present CEB in the CEB5 category. ASTM C62-17 (2017) specifies the minimum requirements of solid masonry made of compacted clay or similar materials, sintered at high temperatures. Based on this standard, the CEB designed in this research can be classified as a 'MW' grade brick, with the advantage that in the manufacturing process of the block no high temperatures were used for sintering its components. This means that good mechanical properties were achieved with an amount of incorporated energy well below the energy required to fabricate a cooked brick.

3.2 Durability tests

Figure 8 shows images of the evolution of the wetting-drying test, using a total of 7 blocks, following the contents of the UNE 41410 standard. After detailed visual inspection, no significant deterioration was observed after the planned 6 cycles of wetting-drying. This corroborates that the stabilization of the soil and the cementation of its particles was very effective, to the point where the physical integrity of the blocks was not affected by the volume changes intentionally induced by the test.

The ice-thaw test used for BTCs was done based on DIN 18945-47 (2013). The durability assessment of the blocks is very important since they mostly measure the longevity of the

CEB. Moreover, sequential submission to freezing and thawing is one of the most aggressive environmental conditions for this class of compacted earth masonry elements. The humidity lodged in the structure of the compacted piece, at the time of the freezing, generates internal pressure in the pores due to the increase in volume of the frozen water, which can even cause a structural collapse (Jamshidi et al., 2016; Mak et al., 2016). Figure 9 presents the temperature profile used during the test, comprising a total of 15 cycles. The exposed surface of the block was moistened and submitted to the temperature variations. At the end of the 15 cycles, no significant damage was observed, including gaps, cracks, fractures or delamination of the material, demonstrating that the structure of the stabilized CEB was strong enough to withstand the stresses caused by the internal pressure of the frozen water during the test.

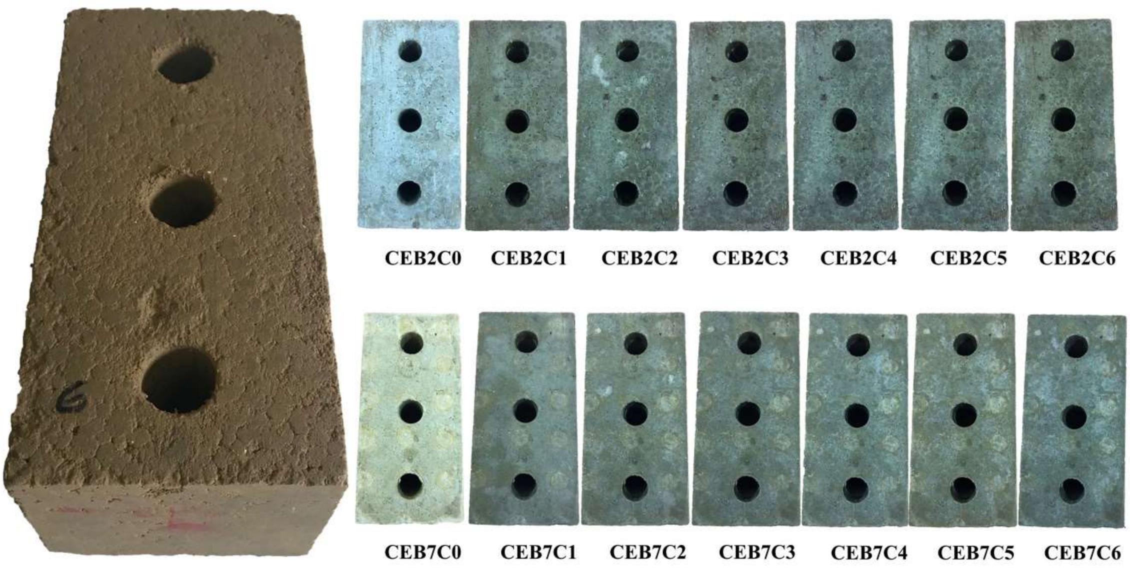

Figure 8. Evolution of two different CEB specimens submitted to the wetting and drying durability test cycles

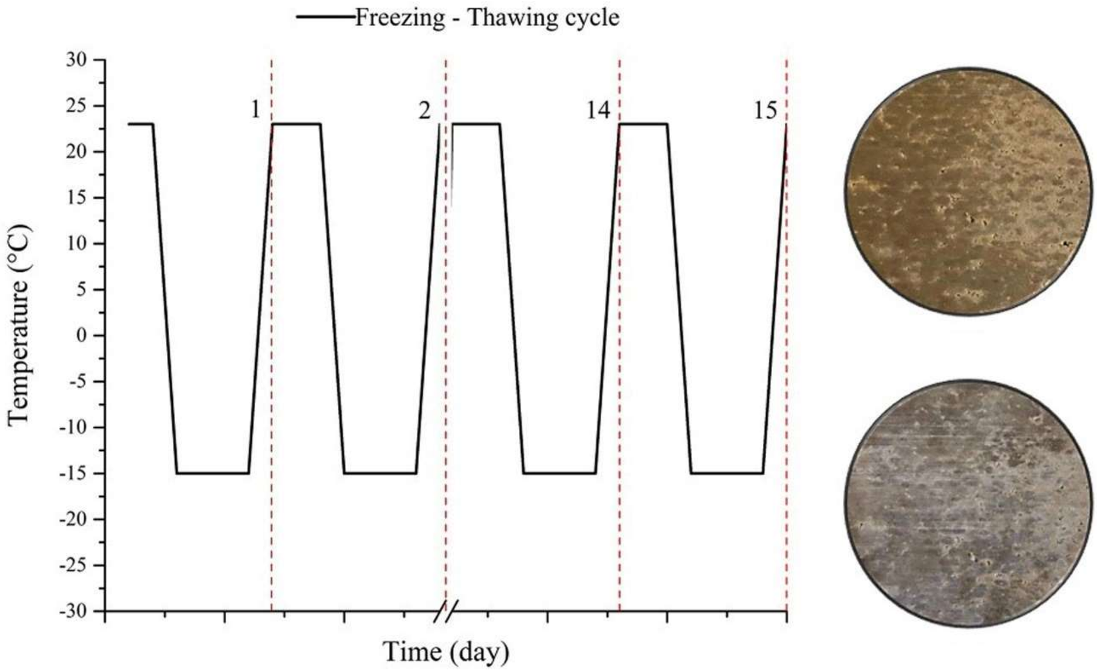

Figure 9. Freeze-thaw temperature cycles

The durability of the CEBs was also evaluated through their resistance to water erosion, tested according to the Swinburne test (SAET), as established in the Spanish standard UNE 41410 (2008). This test was specifically developed for earthen materials and simulates the accelerated erosion action of hitting rain. The test setup consists of a deposit, elevated 1 m above the exposed surface of the CEB, which continuously drops water on the surface of the CEB from an outlet of 5 mm diameter, while keeping a constant water head of 0.5 m (Figure 10a). The surface of the CEB is inclined 27º relatively to the horizontal plane. The water dropping lasts 10 minutes, after which the specimen is opened and the pitting depth caused by the water stream is measured, using a 3 mm diameter probe. According to the contents of the mentioned standard, the CEBs are suitable if the pitting depth is not higher than 10 mm.

The results of the three specimens tested are presented in Table 5. As can be seen in Figure 10b, the water stream did not cause any surface degradation, meaning that the stabilisation solution used is highly effective in providing water erosion resistance to the CEBs. The moisture penetration depth was additionally measured, by breaking the specimens into 2 halves along the longitudinal section hit by the stream (Figure 10b). An average value of 9 mm was observed, although all specimens showed some variation in the penetration depth (Figure 10c), which was caused by the presence of some clogs formed during the mix located near the surface, facilitating the water intake.

Figure 10. Swinburn test setup (a); surface of the CEB after exposure (b); water penetration depth (c)

Table 5. Results of the Swinburn test (CoV in brackets)

Specimen	Pitting depth (mm)	Moisture penetration depth (mm)
S1	0	9
S2	0	10

S3	0	8
Average	0	9 (16%)

3.3 FTIR

Figure 11 shows the IR spectra of the raw material with which the CEBs were manufactured. The FA and WG residues have several signals in common – bands centred around 455, 774 and 776 cm^{-1}, associated with Si-O (quartz) functional groups. The main band of the FA is located around 1023 cm^{-1}, characteristic of Si-O-T (T = Al, Si) type links. This spectrum is typical of a material rich in aluminosilicates (Criado et al., 2007; Gao et al., 2014; Panias et al., 2007; Rivera et al., 2019). The GW has a main band centred around 959 cm^{-1}, and the signals located between 950 - 1000 cm^{-1} are associated with vibration modes of Si-O-Na functional groups in condensed units of type Q2 and Q3 silicates, typical of a calcium sodium glass (Khalil et al., 2010; Rivera et al., 2018; Varma et al., 2009; Véron et al., 2013). The characteristic spectrum of the soil reveals signals at 455 cm^{-1}, 748 cm^{-1} and 998 cm^{-1} wave lengths, associated with vibration modes of Si-O-Si and Si-O functional groups (i.e. quartz). The band signal around 529 cm^{-1} can be attributed to stretching vibrations of Fe-O, Fe2O3 and Si-O-Al type bonds, while bands in the region 850-950 cm^{-1} are characteristic of O-H-Al type links, and the band identified at 1633 cm^{-1} is attributed to bending vibration modes of O-H-O type bonds of water molecules (Kaufhold et al., 2012; Nayak and Singh, 2007; Saikia and Parthasarathy, 2010).

The cleaning solution, being a highly alkaline aqueous solution contaminated by the aluminium foundry industry, is basically composed by products from the reaction between caustic soda and aluminium waste. In its IR spectrum, a signal centred at 527 cm^{-1} can be observed, attributed to non-condensed octahedral species of AlO6 (these octahedral species can present signals between 400 - 530 cm^{-1}). The region between 700 - 900 cm^{-1} is characteristic of AlO4 tetrahedral species (Tarte, 1967). Therefore, it is not surprising that ionic species of $Al(OH)^{-4}$ aluminates in solution were identified in this same region. These aluminate species are predominant in pH values between 8-12, with vibrations of Al-OH type bonds (Li et al., 2014; MA et al., 2007). According to Ram (2001), the bands in the IR spectrum of the cleaning solution around 1019 and 1420 cm^{-1} could be considered as vibration signals of double bond stretching of Al=O of amorphous compounds. In short, and as expected, signals of aluminate compounds and aluminium hydroxides were found in the spectrum of the cleaning solution.

When stabilizing the soil-FA-GW mixture with the cleaning solution, some changes in the IR spectrum of the stabilized material were noted. The cleaning solution, being highly alkaline (pH between 12-14), attacks the amorphous acid oxides included in the precursor materials (FA and GW), and even oxides such as FeO and Fe_2O_3 can be affected by the alkaline attack (Lemougna et al., 2013; Lloyd et al., 2009; van Deventer et al., 2007). Some signals are preserved, such as those from the crystalline quartz 455 cm^{-1}.

On the other hand, bands around 643 and 689 cm-1 can be attributed to new reaction products. According to Criado et al. (2007), in the region between 500 - 800 cm^{-1} the typical signals of various cyclic structures of aluminosilicates formed by the union of SiO4 and AlO4 tetrahedra, linked by oxygen atoms resulting from the alkaline attack, are identified. The compounds identified in the cleaning solution apparently now form part of the new structure of the cementing gel, since the signals of the $Al(OH)^{-4}$ aluminates and AlO_4 tetrahedra are not noticeable in the new stabilized material, and even the signal identified as representing the Al=O link (1425 cm^{-1}) has decreased almost until disappearing. The main band of the stabilized material located around 967 cm^{-1}, can represent different types of overlapping links and structures. Generally the region between 950-1250 cm^{-1} of the FTIR spectrum corresponds to Si-O-T type bonds (T = Si, Al) which indicates that the main reaction product generated by the dissolution of the precursors is an aluminosilicate gel. This region is also related to signals from reactive terminals of the type Si-O-Na plus whichever ions are responsible for generating the aluminosilicate chains (Lee and Van Deventer, 2003). The precise location of the band in this region will depend on the type of generated structure, of alkaline activator used and of the composition of the binding gel (Criado et al., 2007).

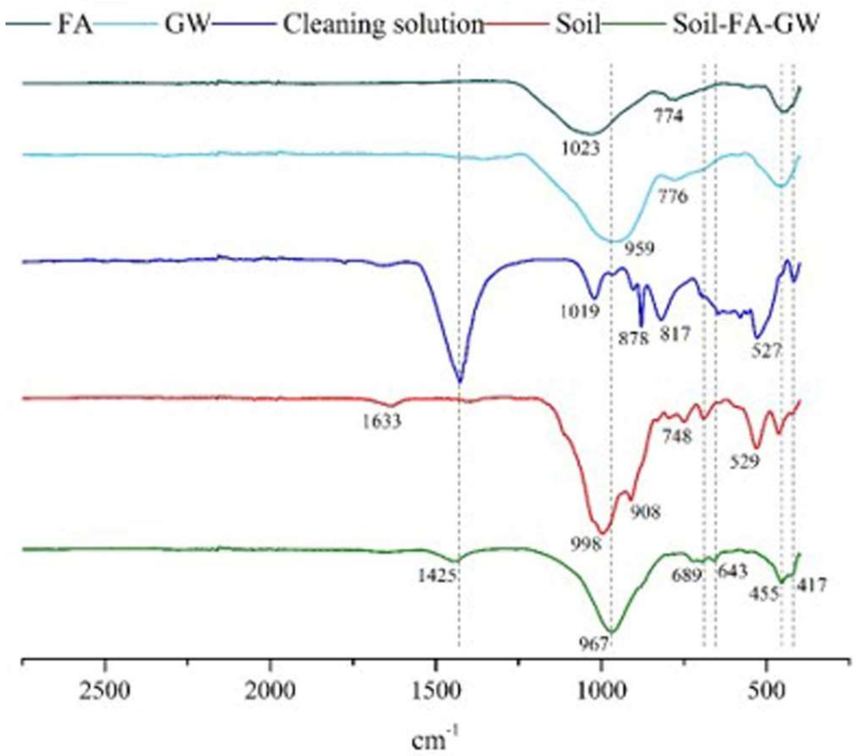

Figure 11. FT-IR spectra of the original and stabilised materials

3.4 SEM

The microstructure of the stabilized soil was examined with scanning electron microscopy, complemented with energy dispersive spectroscopy, for chemical assessment of the binding gel developed. Some of the images obtained (the analysis was performed on a sample collected from one of the previously tested CEBs) are presented in Figure 12, showing the overall morphology of the stabilised soil (Figure 12a), where the binding effect of the material synthesized from alkaline activated residues is clear, resulting in a homogeneous and fairly compacted structure with apparently well cemented soil particles. Figure 12b presented the cemented soil particles in higher detail, where it is possible to detect both precursor and soil particles embedded in what appears to be the cementitious matrix. The nature of the reaction products was identified as a sodium aluminosilicate gel (N-A-S-H), which corroborates the characterization done with FTIR. Indeed, it was previously proposed that the nature of the reaction products was a sodium aluminosilicate gel, due to the nature of the precursors and the alkaline activator.

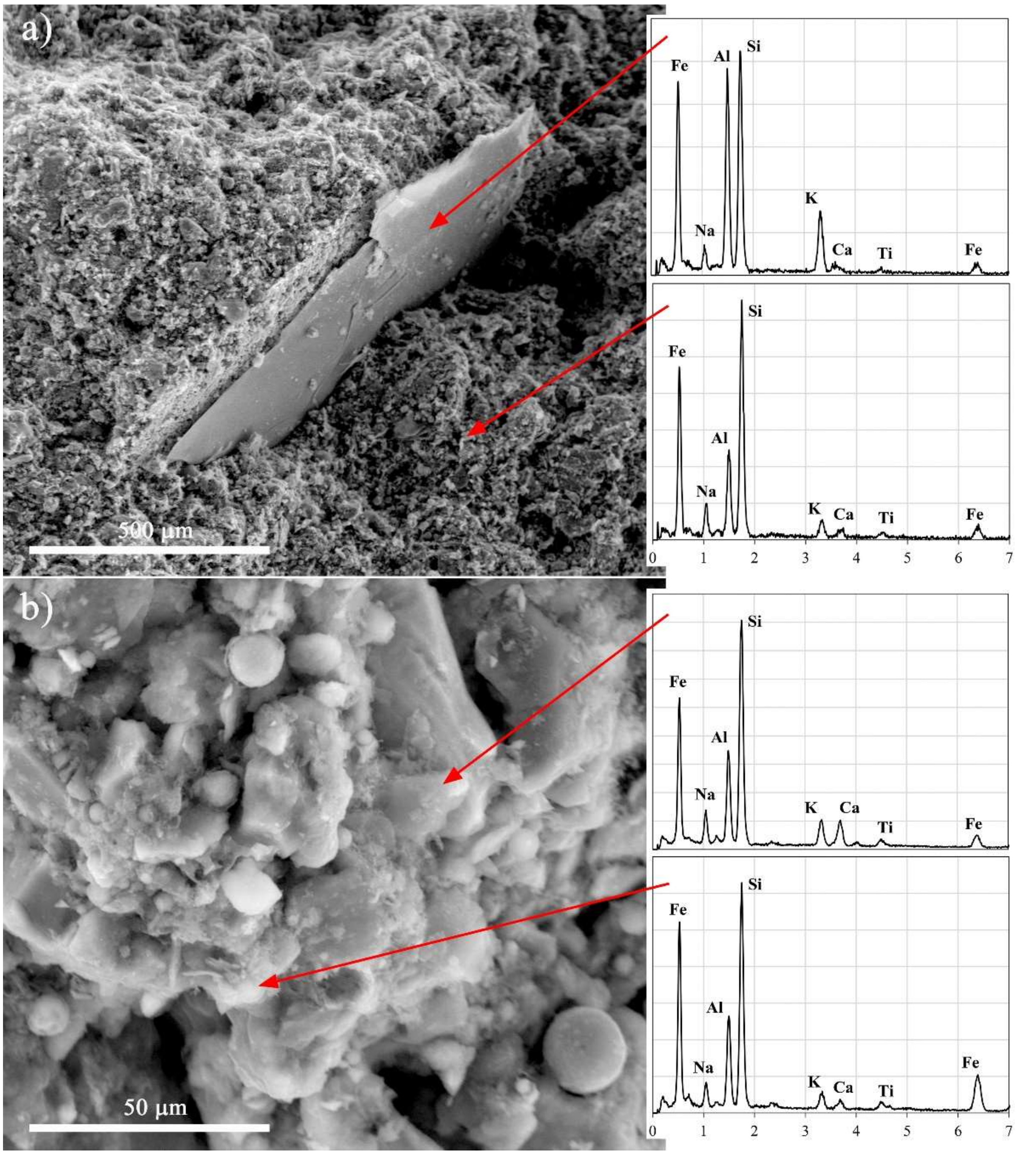

Figure 12. SEM micrographs of the CEB structure

4. Conclusions

This research work demonstrated the viability of alternative and environmentally friendly soil stabilisation, with the specific purpose of manufacturing masonry elements commonly known as “compressed earth blocks”, or CEBs. The alternative synthesized cements are

100% based on industrial waste, and its applicability to soil stabilisation was thoroughly assessed through strength and durability tests. The results showed that such material can be an effective alternative to traditional chemical stabilisation of soils, namely to calcium-based cements, such as lime or Portland cement. The manufacture of compacted earth masonry elements using this type of cementitious material suggests both a technical and environmental advantage since, in theory, the amount of incorporated energy in waste-based binding agents is significantly lower than the energy associated with traditional binders. However, and in order to fully corroborate this, it will be necessary to perform a comparison between both types of binders, in order to characterised and make evident and all the advantages and disadvantages.

Acknowledgments

The authors would also like to acknowledge the contribution of the Electronic Microscopy Unit of the University of Trás-os-Montes e Alto Douro (Dr. Lisete Fernandes), for the microstructural analysis.

Funding

This work was funded by the R&D Project JUSTREST- Development of Alkali Binders for Geotechnical Applications Made Exclusively from Industrial Waste, with reference

PTDC/ECM-GEO/0637/2014, financed by the Foundation for Science and Technology - FCT/MCTES (PIDDAC).

The research was supported by the GEO-DESIGN project, nº17501, co-financed by the European Regional Development Fund (ERDF) through NORTE 2020 (North Regional Operational Program 2014/2020).

References

ASTM C618, 2012. Standard specification for coal fly ash and raw or calcined natural pozzolan for use in concrete. ASTM Int. Annu. B. Stand. 1–5.

ASTM C62-17, 2017. Standard Specification for Building Brick (Solid Masonry Units Made From Clay or Shale). Am. Soc. Test. Mater.

Avila-López, U., Almanza-Robles, J.M., Escalante-García, J.I., 2015. Investigation of novel waste glass and limestone binders using statistical methods. Constr. Build. Mater. 82, 296–303.

Bakharev, T., 2005. Geopolymeric materials prepared using Class F fly ash and elevated temperature curing. Cem. Concr. Res. 35, 1224–1232.

BSi EN 13286-53, 2004. Unbound and hydraulically bound mixtures. Method for the manufacture of test specimens of hydraulically bound mixtures using axial compression. Br. Stand. Institution, London.

Corrêa-Silva, M., Araújo, N., Cristelo, N., Miranda, T., Gomes, A.T., Coelho, J., 2019. Improvement of a clayey soil with alkali activated low-calcium fly ash for transport infrastructures applications. Road Mater. Pavement Des. 20, 1912–1926.

Criado, M., Fernández-Jiménez, A., Palomo, A., 2010. Alkali activation of fly ash. Part III: Effect of curing conditions on reaction and its graphical description. Fuel 89, 3185–3192.

Criado, M., Fernández-Jiménez, A., Palomo, A., 2007. Alkali activation of fly ash: Effect of the SiO2/Na2O ratio. Microporous Mesoporous Mater. 106, 180–191.

Cristelo, N., Fernández-Jiménez, A., Castro, F., Fernandes, L., Tavares, P., 2019. Sustainable alkaline activation of fly ash, aluminium anodising sludge and glass powder blends with a recycled alkaline cleaning solution. Constr. Build. Mater. 204, 609–620.

Cristelo, N., Fernández-Jiménez, A., Vieira, C., Miranda, T., Palomo, Á., 2018. Stabilisation of construction and demolition waste with a high fines content using alkali activated fly ash. Constr. Build. Mater. 170, 26–39.

DIN 18945-47, 2013. Earth blocks - terms, requirements, test methods. DIN Stand.

El-Mahllawy, M.S., Kandeel, A.M., Latif, M.L.A., El Nagar, A.M., 2018. The feasibility of using marble cutting waste in a sustainable building clay industry. Recycling 3, 39.

Espinoza, L.J., Escalante García, I., 1970. Morteros a base de vidrio de desecho/escoria de alto horno; activación mecanoquímica del vidrio en soluciones alcalinas. Nexo Rev. Científica 24, 92–103.

Fernández-Jiménez, A., Cristelo, N., Miranda, T., Palomo, Á., 2017. Sustainable alkali activated materials: Precursor and activator derived from industrial wastes. J. Clean. Prod. 162, 1200–1209.

Fernández-Jiménez, A., Monzó, M., Vicent, M., Barba, A., Palomo, A., 2008. Alkaline activation of metakaolin-fly ash mixtures: Obtain of Zeoceramics and Zeocements. Microporous Mesoporous Mater. 108, 41–49.

Fernández-Jiménez, A., Palomo, A., Sobrados, I., Sanz, J., 2006. The role played by the reactive alumina content in the alkaline activation of fly ashes. Microporous Mesoporous Mater. 91, 111–119.

Gao, K., Lin, K.L., Wang, D., Hwang, C.L., Shiu, H.S., Chang, Y.M., Cheng, T.W., 2014. Effects SiO2/Na2O molar ratio on mechanical properties and the microstructure of nano-SiO2 metakaolin-based geopolymers. Constr. Build. Mater. 53, 503–510.

Horpibulsuk, S., Rachan, R., Raksachon, Y., 2009. Role of fly ash on strength and microstructure development in blended cement stabilized silty clay. Soils Found. 49, 85–98.

Hwang, J.-Y., Huang, X., Garkida, A., Hein, A., 2006. Waste Colored Glasses as Sintering

Aid in Ceramic Tiles Production. J. Miner. Mater. Charact. Eng. 05, 119–129.
Jamshidi, A., Nikudel, M.R., Khamehchiyan, M., 2016. Evaluation of the durability of Gerdoee travertine after freeze-thaw cycles in fresh water and sodium sulfate solution by decay function models. Eng. Geol. 202, 36–43.
Kaufhold, S., Hein, M., Dohrmann, R., Ufer, K., 2012. Quantification of the mineralogical composition of clays using FTIR spectroscopy. Vib. Spectrosc. 59, 29–39.
Khalil, E.M.A., ElBatal, F.H., Hamdy, Y.M., Zidan, H.M., Aziz, M.S., Abdelghany, A.M., 2010. Infrared absorption spectra of transition metals-doped soda lime silica glasses. Phys. B Condens. Matter 405, 1294–1300.
Lee, W.K.W., Van Deventer, J.S.J., 2003. Use of Infrared Spectroscopy to Study Geopolymerization of Heterogeneous Amorphous Aluminosilicates. Langmuir 19, 8726–8734.
Leitão, D., Barbosa, J., Soares, E., Miranda, T., Cristelo, N., Briga-Sá, A., 2017. Thermal performance assessment of masonry made of ICEB’s stabilised with alkali-activated fly ash. Energy Build. 139, 44–52.
Lemougna, P.N., MacKenzie, K.J.D., Jameson, G.N.L., Rahier, H., Chinje Melo, U.F., 2013. The role of iron in the formation of inorganic polymers (geopolymers) from volcanic ash: A 57Fe Mössbauer spectroscopy study. J. Mater. Sci. 48, 5280–5286.
Li, X. Bin, Zhao, D.F., Yang, S.S., Wang, D.Q., Zhou, Q.S., Liu, G.H., 2014. Influence of thermal history on conversion of aluminate species in sodium aluminate solution. Trans. Nonferrous Met. Soc. China (English Ed. 24, 3348–3355.
Lima, S.A., Varum, H., Sales, A., Neto, V.F., 2012. Analysis of the mechanical properties of compressed earth block masonry using the sugarcane bagasse ash. Constr. Build. Mater. 35, 829–837.
Lin, K.L., Shiu, H.S., Shie, J.L., Cheng, T.W., Hwang, C.L., 2012. Effect of composition on characteristics of thin film transistor liquid crystal display (TFT-LCD) waste glass-metakaolin-based geopolymers. Constr. Build. Mater. 36, 501–507.
Lloyd, R.R., Provis, J.L., Van Deventer, J.S.J., 2009. Microscopy and microanalysis of inorganic polymer cements. 1: Remnant fly ash particles. J. Mater. Sci. 44, 608–619.
MA, S. hua, ZHENG, S. li, XU, H. bin, ZHANG, Y., 2007. Spectra of sodium aluminate solutions. Trans. Nonferrous Met. Soc. China (English Ed. 17, 853–857.

Mak, K., MacDougall, C., Fam, A., 2016. Freeze-thaw performance of on-site manufactured compressed earth blocks: Effect of water repellent and other additives. J. Mater. Civ. Eng. 28, 04016034.

Miranda, T., Silva, R.A., Oliveira, D. V., Leitão, D., Cristelo, N., Oliveira, J., Soares, E., 2017. ICEBs stabilised with alkali-activated fly ash as a renewed approach for green building: Exploitation of the masonry mechanical performance. Constr. Build. Mater. 155, 65–78.

Montgomery, D.C., Runger, G.C., 2014. Applied Statistics and Probability for Engineers, Sixth Edit. ed, Blood Pressure.

Nayak, P.S., Singh, B.K., 2007. Instrumental Characterization of Clay by FTIR, XRF, BET and, TPD-NH3. Bull. Mater. Sci. 30, 235–238.

Novais, R.M., Ascensão, G., Seabra, M.P., Labrincha, J.A., 2016. Waste glass from end-of-life fluorescent lamps as raw material in geopolymers. Waste Manag. 52, 245–255.

Olufowobi, J., Ogundoju, A., Michael, B., Aderinlewo, O., 2014. Clay soil stabilisation using powdered glass. J. Eng. Sci. Technol. 9, 541–558.

Omar Sore, S., Messan, A., Prud'homme, E., Escadeillas, G., Tsobnang, F., 2018. Stabilization of compressed earth blocks (CEBs) by geopolymer binder based on local materials from Burkina Faso. Constr. Build. Mater. 165, 333–345.

Oti, J.E., Kinuthia, J.M., Bai, J., 2009a. Compressive strength and microstructural analysis of unfired clay masonry bricks. Eng. Geol. 109, 230–240.

Oti, J.E., Kinuthia, J.M., Bai, J., 2009b. Engineering properties of unfired clay masonry bricks. Eng. Geol. 107, 130–139.

Pacheco-Torgal, F., Jalali, S., 2012. Earth construction: Lessons from the past for future eco-efficient construction. Constr. Build. Mater.

Panias, D., Giannopoulou, I.P., Perraki, T., 2007. Effect of synthesis parameters on the mechanical properties of fly ash-based geopolymers. Colloids Surfaces A Physicochem. Eng. Asp. 301, 246–254.

Pascual, A.B., Tognonvi, M.T., Tagnit-hamou, A., 2014. WASTE GLASS POWDER-BASED ALKALI-ACTIVATED MORTAR. Int. J. Res. Eng. Technol. 03, 32–36.

Ram, S., 2001. Infrared spectral study of molecular vibrations in amorphous, nanocrystalline and AlO(OH) · αh2O bulk crystals. Infrared Phys. Technol. 42, 547–

560.
Rios, S., Cristelo, N., da Fonseca, A.V., Ferreira, C., 2016. Structural performance of alkali-activated soil ash versus soil cement. J. Mater. Civ. Eng. 28.
Rivera, J.F., Cristelo, N., Fernández-Jiménez, A., Mejía de Gutiérrez, R., 2019. Synthesis of alkaline cements based on fly ash and metallurgic slag: Optimisation of the SiO_2/Al_2O_3 and Na_2O/SiO_2 molar ratios using the response surface methodology. Constr. Build. Mater. 213, 424–433.
Rivera, J.F., Cuarán-Cuarán, Z.I., Vanegas-Bonilla, N., Mejía de Gutiérrez, R., 2018. Novel use of waste glass powder: Production of geopolymeric tiles. Adv. Powder Technol. 29, 3448–3454.
Ryu, G.S., Kim, S.H., Koh, K.T., Kang, S.T., Lee, J.H., 2012. Influence of curing temperature on the mechanical properties of alkali-activated bottom ash geopolymer mortar, in: Key Engineering Materials. pp. 198–201.
Saikia, B.J., Parthasarathy, G., 2010. Fourier Transform Infrared Spectroscopic Characterization of Kaolinite from Assam and Meghalaya, Northeastern India. J. Mod. Phys. 01, 206–210.
Siddiqua, S., Barreto, P.N.M., 2018. Chemical stabilization of rammed earth using calcium carbide residue and fly ash. Constr. Build. Mater. 169, 364–371.
Silva, R. a, Soares, E., Oliveira, D. V., Miranda, T., Cristelo, N., Leitão, D., 2015. Mechanical characterisation of dry-stack masonry made of CEBs stabilised with alkaline activation. Constr. Build. Mater. 75, 349–358.
Šimonová, H., Keršner, Z., Schmid, P., Rovnaníková, P., 2018. Effect of curing temperature on mechanical and fracture parameters of alkali-activated brick powder based composite, in: Key Engineering Materials. pp. 79–82.
Singh, G.V.P.B., Subramaniam, K.V.L., 2019. Influence of processing temperature on the reaction product and strength gain in alkali-activated fly ash. Cem. Concr. Compos. 95, 10–18.
Tarte, P., 1967. Infra-red spectra of inorganic aluminates and characteristic vibrational frequencies of AlO_4 tetrahedra and AlO_6 octahedra. Spectrochim. Acta 23A, 2127–2143.
Torres-Carrasco, M., Palomo, J.G., Puertas, F., 2014. Sodium silicate solutions from

dissolution of glasswastes. Statistical analysis. Mater. Constr. 64, e014.

Torres-Carrasco, M., Puertas, F., 2015. Waste glass in the geopolymer preparation. Mechanical and microstructural characterisation. J. Clean. Prod. 90, 397–408.

UNE 41410, 2008. UNE 41410:2008 - Bloques de tierra comprimida para muros y taboques/Definiciones, especificaciones y métodos de ensayo. AENOR - Asoc. Española Norm. y Certificación 28.

van Deventer, J.S.J., Provis, J.L., Duxson, P., Lukey, G.C., 2007. Reaction mechanisms in the geopolymeric conversion of inorganic waste to useful products. J. Hazard. Mater. 139, 506–513.

Varma, R.S., Kothari, D.C., Tewari, R., 2009. Nano-composite soda lime silicate glass prepared using silver ion exchange. J. Non. Cryst. Solids 355, 1246–1251.

Véron, O., Blondeau, J.P., Meneses, D.D.S., Vignolle, C.A., 2013. Characterization of silver or copper nanoparticles embedded in Soda-lime glass after a staining process. Surf. Coatings Technol. 227, 48–57.

Zhang, Z., Wong, Y.C., Arulrajah, A., Horpibulsuk, S., 2018. A review of studies on bricks using alternative materials and approaches. Constr. Build. Mater.